Since January 2020 Elsevier has created a COVID-19 resource centre with free information in English and Mandarin on the novel coronavirus COVID-19. The COVID-19 resource centre is hosted on Elsevier Connect, the company's public news and information website.

Talanta 262 (2023) 124701

Contents lists available at ScienceDirect

Talanta

journal homepage: www.elsevier.com/locate/talanta

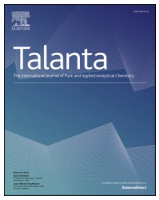

Synthesis and characterization of Au-decorated graphene oxide nanocomposite for magneto-electrochemical detection of SARS-CoV-2 nucleocapsid gene

Pravanjan Malla [a], Chi-Hsien Liu [a,b,c,*], Wei-Chi Wu [c,d], Pinpinut Kabinsing [a], Paiboon Sreearunothai [e,**]

[a] Department of Chemical and Materials Engineering, Chang Gung University, 259, Wen-Hwa First Road, Tao-Yuan, Taiwan
[b] Research Center for Chinese Herbal Medicine and Research Center for Food and Cosmetic Safety, College of Human Ecology, Chang Gung University of Science and Technology, 261, Wen-Hwa First Road, Taoyuan, Taiwan
[c] Department of Ophthalmology, Chang Gung Memorial Hospital, Linkou, 5, Fu-Hsing Street, Taoyuan, Taiwan
[d] College of Medicine, Chang Gung University, 259, Wen-Hwa First Road, Taoyuan, Taiwan
[e] Sirindhorn International Institute of Technology, Thammasat University, Pathum Thani, Thailand

ARTICLE INFO

Handling Editor: J.-M. Kauffmann

Keywords:
Genosensor
CoV-2
Nucleocapsid gene
Electrochemical biosensor
Reduced graphene oxide

ABSTRACT

Fast and effective diagnosis is the first step in monitoring the current coronavirus 2 (CoV-2) pandemic. Herein, we establish a simple and sensitive electrochemical assay using magnetic nanocomposite and DNA sandwich probes to rapidly quantify the CoV-2 nucleocapsid (N) gene down to the 0.37 fM level. This assay uses a pair of specific DNA probes. The capture probe is covalently conjugated to Au-decorated magnetic reduced graphene oxide (AMrGO) nanocomposite for efficiently capturing target RNA. In contrast, the detection probe is linked to peroxidase for signal amplification. The probes target the COV-2 gene, allowing for specific magnetic separation, enzymatic signal amplification, and subsequent generation of voltammetric current with a total assay time of 45 min. The developed biosensor has high selectivity and can discriminate non-specific gene sequences. Synthetic COV-2 N-gene can be detected efficiently in serum and saliva, while 1-bp mismatch gene yielded a low response. The performance of the genosensor was good in an extensive linear range of 5 aM–50 pM. For synthetic N-gene, we achieved the detection limit of 0.37, 0.33, and 0.19 fM in human saliva, urine, and serum. This simple, selective, and sensitive genosensor could have various genetics-based biosensing and diagnostic applications.

1. Introduction

The mutation of severe acute respiratory syndrome coronavirus 2 (SARS-CoV-2) has made correct and quick diagnosis difficult. Developing efficient detection for SARS-CoV-2 is crucial for mitigating the pandemic. Rapid and straightforward determination of unique RNA/DNA sequences from a small amount of a viral pathogen is in great demand [1]. The reverse transcription polymerase chain reaction (PCR) is the standard for diagnosing and confirming a viral infection, using the gene as the target. However, the significant disadvantages of PCR were the time it takes in thermal cycling amplification of the target gene to reach the detectable level, the complication associated with the thermal cycling equipment, and the cost of the reagents involved. Electrochemical detection-based gene sensors are an attractive alternative as they may provide a more rapid, lower price, and simpler control than the PCR [2].

Point-of-care diagnostic devices aim to develop plug-and-play detection to manage the SARS-CoV-2 outbreak and prevent future epidemics [3,4]. Antibody/antigen-based methods also have been developed for diagnosing body response proteins. For example, an enzyme-linked immunosorbent assay and lateral flow immunoassay can detect specific proteins that the body produces, which could be several days after the infection [5]. These immunoassays have the limitations that the antibodies are expensive, and there can be a significant deviation in detection. Electrochemical analyses are increasingly being used as rapid tests since this methodology provides a straightforward

* Corresponding author. Department of Chemical and Materials Engineering, Chang Gung University, 259, Wen-Hwa First Road, Tao-Yuan, Taiwan.
** Corresponding author.
E-mail addresses: CHL@mail.cgu.edu.tw (C.-H. Liu), paiboon@siit.tu.ac.th (P. Sreearunothai).

https://doi.org/10.1016/j.talanta.2023.124701
Received 30 January 2023; Received in revised form 17 May 2023; Accepted 22 May 2023
Available online 23 May 2023

and cheap arrangement due to the possibility of a label-free detection [6]. For this purpose, electrochemical genosensors combine the inherent specificity of Watson–Crick base-pairing with the high sensitivity of electrochemical sensors and thus sustain the development of the next generation of POC tests.

Electrochemical genosensors employing nanomaterials could provide detection with several benefits, such as great sensitivity and selectivity, early detection, celerity, and low-cost [7,8]. Reduced graphene oxide (rGO) advantages include a large specific surface area, high conductivity, and good stability [9]. However, its tendency to stack and aggregate can be detrimental to diagnostic applications that try to utilize its large surface area [10]. Decorating metal or metal oxide nanoparticles onto rGO sheets can reduce stacking and impart other desirable properties. Combining different nanomaterials on the electrode may provide synergic advantages such as improved catalytic, magnetic, and electrical properties [11,12]. For example, graphene decorated with gold nanoparticles (AuNP) can catalyze tetramethylbenzidine oxidation in hydrogen peroxide [13].

The gold nanoparticles can enhance the sensitivity of electrochemical sensors because of their excellent conductivity and catalyst activity [14]. This Au-graphene nanocomposite conjugated with an antibody has been reported to detect noroviruses in the human serum [15]. Au-doped magnetic nanoparticles (MNP) combined with rGO have been used in the DNA sensor to detect the genetically modified plant synthase gene [16]. AuNP-rGO combined with horseradish peroxidase (HRP) labeled MNP was employed to investigate the caspase activity assay in the apoptotic phase of lung cancer cells using an engineered peptide and electrochemiluminescence [14]. DNA biosensors for detecting human T-lymphotropic viruses have been developed using rGO-polypyrrole-AuNPs and differential pulse voltammetry (DPV) technique [17]. This specific DNA probe immobilized on a nanocomposite can capture the target DNA and activate the electrochemical oxidation of the electron transfer mediator anthraquinone [17]. The large surface area of reduced graphene oxide, combined with the catalytic activity of gold nanoparticles can offer a synergetic advantage for grating gene-capturing probes, enabling a large number of target genes or RNA to be captured.

MNPs have several attractive properties: ease of synthesis, versatile modification, good stability, and the ability for rapid magnetic separation and enrichment. MNP grafted with capture ligand can be used to specifically capture target DNA from solution and quickly separated from the media onto the electrochemical electrode using a magnet [18]. In addition, MNPs can increase the electrode's area, roughness, and porosity and enhance the sensor's sensitivity. For example, electrochemical reactions catalyzed by HRP-modified MNP provide better signals using the magnet to attract the MNP close to the electrode than freely suspended nanoparticles [19]. The electrochemical signal is improved because of the shorter distance for electron transfer by keeping the redox reaction in proximity to the electrodes using the MNP's superparamagnetic property [20]. However, MNP itself tends to have a small surface area. Hence the use of Au-rGO as a platform for immobilization of the capture probes, combined with MNP for rapid magnetic separation and enrichment of the targets onto the electrochemical sensing electrode, can provide an attractive strategy for ultrasensitive magneto-electrochemical detection of the target gene.

The N protein is present in multiple copies of the viral particle and is one of the most popular targets in the COVID diagnosis. However, the spike (S) protein is more vulnerable to mutation than the N protein [21]. Therefore, it is crucial to choose conserved regions within structural proteins less prone to mutation. For example, Agarwal et al. demonstrated that most lateral flow assays utilize N protein which has not undergone significant mutational changes [22]. On the other hand, the viral S protein has evolved in recent months through mutations, and some variants may escape neutralizing antibodies from the vaccine [23]. Therefore, it is crucial to choose conserved regions within structural proteins less prone to mutation.

Furthermore, the N gene has less nucleotide variation than ORF1ab may make the detection of the N gene more stable than ORF1ab, which could partially explain why the N gene, rather than ORF1ab, as suggested by Zhang et al. [24]. Therefore, the N gene is used as a model gene to prove the concept in this study.

We present a low-cost electrochemical genosensor based on a screen-printed electrode (SPE) and Au-decorated magnetic reduced graphene oxide (AMrGO) for nucleocapsid (N) gene detection using capture/detection oligonucleotide probes combined with square wave voltammetry. The detection or the reporting probe was linked with the horseradish peroxidase enzyme for signal amplification with hydrogen peroxide and anthraquinone. The specific Watson–Crick base-pairing between the capture probe and target gene sequence is the mechanism used to detect the viral N-gene (Fig. 1). We systematically characterized the nanocomposite and evaluated the RNA biosensor using mismatch sequences from the N gene.

2. Experimental section

2.1. Materials and synthesis of AMrGO

Extra pure chemicals were used without further purification in this study. The detailed sequences of the oligonucleotides are displayed in Table S1. For the synthesis of graphene oxide, we used the improved Hummers' method [25]. The synthesis of AMrGO is performed according to the previous paper [26]. An aliquot of 400 μL AMrGO (1 mg mL^{-1}) was washed twice using 1 mL of 0.1 M, pH 7 PBS, and the precipitate was collected using a magnet. The AMrGO in a 1.5 mL tube was activated using a cross-linker EDC/NHS. Briefly, 200 μL (25.6 mg/200 μL) of EDC and 200 μL (51.2 mg/200 μL) of NHS were added to the tube. The tubes were vortex for 60 min, and AMrGO was washed twice with phosphate solution. Then 0.25 μM of capture probe (Cp) was added to the tube and allowed to vortex for 60 min at room temperature. After 30 min, the supernatant was discarded, and the modified AMrGO/Cp was washed twice using a phosphate solution. After that, 3% BSA solution was added to the AMrGO/Cp for blocking and incubated for 15 min at room temperature. Finally, the AMrGO/Cp/BSA was suspended with 400 μL of phosphate solution and stored at 4 °C for further use or storage test.

2.2. Detection of synthetic N-gene of SARS-CoV-2

Different concentrations of N-gene were dissolved in human saliva and urine, incubated with AMrGO/Cp/BSA, and vortexed for 15 min for hybridization. The supernatant was discarded and washed twice with 0.1 M phosphate solution. The biotinylated N_3R primer as the detection probe (Dp) was added to the tube and vortex for 15 min at room temperature. After that, the diluted streptavidin-conjugated horseradish peroxidase (SHRP) was added and incubated for 15 min. The nanocomposite was washed with a phosphate solution. Finally, the AMrGO/Cp/BSA/target/Dp/SHRP was suspended in a phosphate solution. The electrochemical measurements were performed using an Autolab workstation.

2.3. Calculation of association constant, surface density, and effective surface area

The association constant (Ka) related to the equilibrium adsorption between N-gene and Cp on AMrGO was determined using EIS data and the assumptions of the Langmuir isotherm [27]. The effective surface area was estimated from CV's peak current (I_P) using Randles-Sevcik equation [28]. The Cp surface density on the nanocomposite surface can be calculated using chronocoulometry and hexaammineruthenium (Ru) as a redox mediator [29].

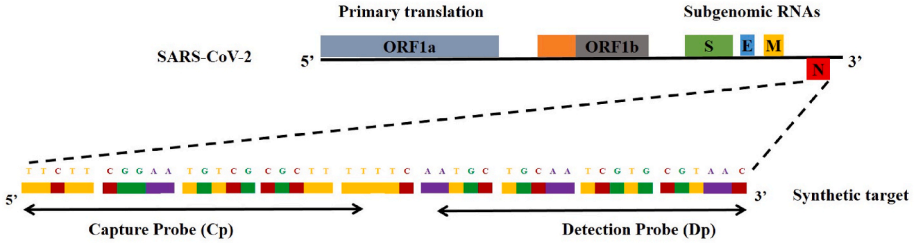

Fig. 1. Illustration of major functional genes of the SARS-CoV-2, the synthetic target N-gene, the capture probe (Cp), and the detection probe (Dp) sequences.

2.4. Optimization of measurement parameters

To optimize the signal and reduce the noise, process factors such as concentrations of Cp, Dp, and SHRP, the incubation time, and hybridization time were evaluated using one aspect at on-time experiments with three repeats. The signal/blank (S/B) ratios were calculated as follows:

$$S/B \text{ ratio} = I_S/I_B$$

Where I_S the signal of nanocomposites in the presence of 500 fM of target RNA or DNA, and I_B is the blank current. The 5.0 mM H_2O_2/5.0 mM HQ solution was used as HRP substrates for SWV analysis. The limit of detection (LOD) was obtained by 3 × standard deviation/sensitivity. All data were reported as means ± standard deviations using Microsoft Excel software. In this work, 5 μL of AMrGO (sample volume) was dropped onto the electrode surface, and an external magnet was placed on the backside of the electrode to attract AMrGO. The SWV signals of AMrGO were obtained by adding 95 μL of 5.0 mM H_2O_2/5.0 mM HQ solution. All the washing steps were followed by using 0.1 M phosphate buffer saline of pH 7.

3. Results

3.1. Principle and fabrication of the genosensor

The detection mechanism and fabrication steps of the developed genosensor for N-gene detection are shown in Fig. 2. First, the aminated capture sequence was immobilized on the carboxylated nanocomposite by EDC/NHS conjugation. After incubation with the N-gene, the biotinylated detection probes were hybridized with N-gene sequences on the magnetic nanocomposite. The SHRP label on the biotinylated double helix can catalyze the substrate and generate a current. Herein, H_2O_2 was a substrate for the SHRP, and HQ was a mediator shuttling electron between the active centers of peroxidase and the working electrode.

By putting a solution of AMrGO and DNA sample to the working electrode with an external magnet, a sensing layer was formed on the SPE for the EIS and DPV assays. Direct modification on the electrode surface was not necessary. AMrGO sensing layer had higher repeatability than direct modification on electrode surface. In addition, the magnetic force of the electrode was easily removed, the wash of electrode was convenient, and the deterioration on electrode surface was reduced. Herein, a disposable SPE covered with a drop of solution containing DNA sample and AMrGO was used as the electrolytic cell for N-gene sensing.

3.2. Characterizations of the modified nanocomposites

3.2.1. Morphology of the nanocolmposite

The SEM technique studied the morphology of modified nanocomposites. Fig. S1(A) shows the flake-like structure of the GO surface, making up the cavity, typically with high roughness. After reducing and magnetizing GO to MrGO, iron oxide particles were observed on the nanosheet in Fig. S1(B). The decoration of Au nanoparticles on AMrGO is shown in Fig. S1(C). The energy dispersive X-ray spectroscopy (EDS)

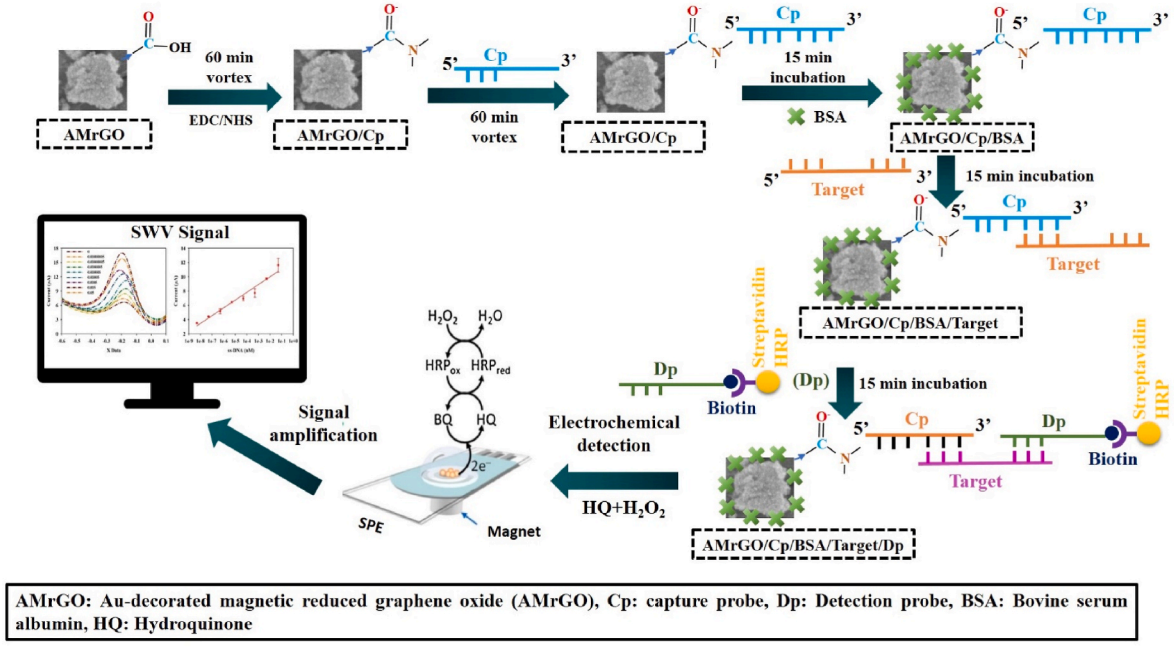

Fig. 2. The procedure of electrochemical detection for the N-gene of SARS-CoV-2.

results indicated that Au and iron elements existed on the rGO. The small dots in Fig. S1(D) represent Au nanoparticles, which enhance conductivity, while the aggregated particles of iron oxide on the flaked surface are seen in Fig. S1(E). In addition, the size of the nanocomposites (MrGO and AMrGO) was characterized using the dynamic light scattering method. An increase in size from 165 nm to 257 nm indicated that magnetic particles had been deposited on the rGO surface. The sizes and zeta potentials are summari zed in Table S2 and Fig. S2. The size increased from 165 nm to 307 nm, and the zeta potential increased from −8 mV to 7 mV when GO was modified to AMrGO.

3.2.2. Raman, TGA, FTIR, and magnetization characterizations

Raman spectroscopy can provide useful information for rGO basal plane structure. Fig. S1 (G) shows the Raman spectra of GO, MrGO, and AMrGO. Each spectrum exhibits a G band around 1600 cm^{-1} corresponding to scattering from in-plane vibrations of the sp^2 carbon atoms and a D band at 1350 cm^{-1} corresponding to scattering from out-of-plane vibrations of the sp^3 carbon atoms. The intensity ratio of these two bands (I_D/I_G) indicates the degree of modification in the nanocomposites. The p-doping effects of Au and iron oxide may hinder the in-plane sp^2 vibration of C═C bonds, increasing the I_D/I_G ratio and shifting the D band slightly [30]. The thermal decomposition of rGO derivatives was investigated using TGA in nitrogen, as shown in Fig. S1(H). GO decomposed rapidly from room temperature to 500 °C, which is expected as graphene oxide was not thermally stable.

In contrast, MrGO and AMrGO, which underwent hydrothermal treatment, were much more thermally stable than GO. AMrGO had a lower decomposition rate than MrGO due to incorporating the thermally more stable Au part in the nanocomposite. The magnetic properties of the magnetic nanocomposites were measured using SQUID, as shown in Fig. S3. The MrGO had greater magnetization than the AMrGO as Au was a paramagnetic material with weak magnetization. However, the magnetization of the AMrGO nanocomposite was about 11 emu/g which was still sufficient for the magnetic attraction onto the SPE electrode. The functional groups on the developed AMrGO were also characterized using Fourier transform Infrared (FTIR) spectroscopy. The existence of iron oxide in MrGO and AMrGO was proved by the characteristic peak of Fe–O (near 630 cm^{-1}) in Fig. S1(I). The stretching vibrations of C–O (1084 cm^{-1}), C═C (1627 cm^{-1}), and O–H (near 3450 cm^{-1}) indicated the existence of GO in MrGO and AMrGO.

3.3. Electrochemical characterizations

The surface modification of AMrGO was also characterized using cyclic voltammetry (CV) and electrochemical impedance spectroscopy (EIS). Before the measurement, the AMrGO was suspended in a 3 mM ferricyanide phosphate solution. As shown in Fig. 3(A), the current changed in different modification steps. The bare SPE surface showed the lowest peak current, gradually increasing after the nanocomposite modification. The peak current of the bare SPE increased from 2.72 μA

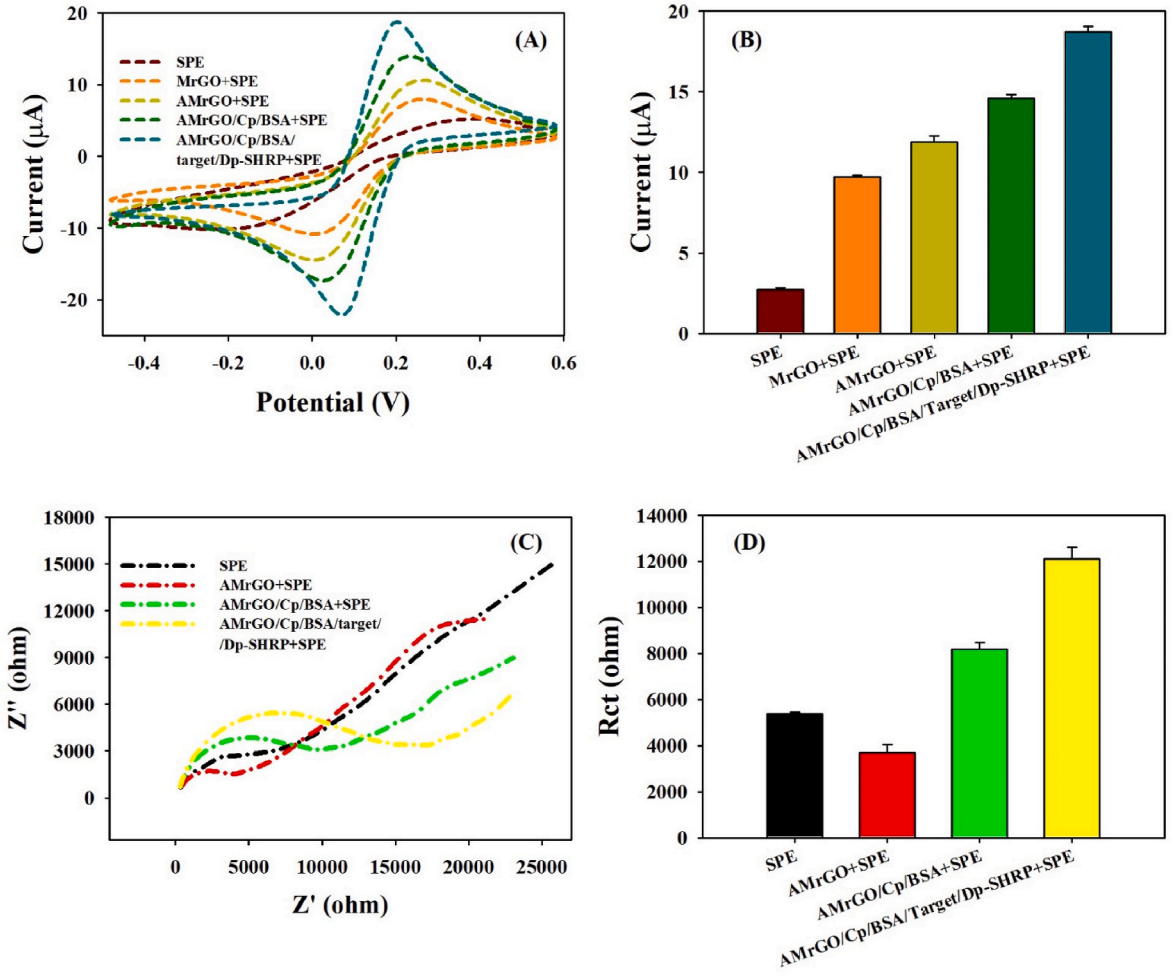

Fig. 3. (A) Cyclic voltammograms of the different AMrGOs, and (B) corresponding anodic peak currents. (C) EIS of the magnetic nanocomposite after successive immobilizations and (D) the corresponding charge transfer resistance of the magnetic nanocomposite. Whereas SPE refers to the screen printed electrode, MrGO: magnetic reduced graphene oxide, AMrGO: Au-decorated magnetic reduced graphene oxide, Cp: capture probe BSA: bovine serum albumin, Target: synthetic N-gene (45 bp), Dp: detection probe, SHRP: streptavidin horseradish peroxidase.

to 18.7 μA after being labeled by SHRP, corresponding to ~ eight times higher than that of bare SPE (Fig. 3(B)).

Furthermore, incubating the modified nanocomposites with the specific capture sequence of SARS-CoV-2 and blocking with BSA led to a further increase in the current. The symmetric peaks of CV in Fig. 3(A) indicate a reversible electrochemical reaction. The peak current in the voltammetry using different scan rates can be used to evaluate the electron transfer rate (Ks) of the electrode–electrolyte–nanocomposite interface. The electron transfer rates of the graphene nanocomposites after layer-by-layer modification were estimated. The decoration of Au on GO increased the Ks from 0.0024 to 0.0039 cm s^{-1}. After conjugating the captured DNA, the Ks increased to 0.005 cm s^{-1}. The decoration of AuNPs on GO has been reported to enhance the kinetics of electron transfer using a redox probe on the electrode [31]. The detailed transfer rates of the nanocomposites are summarized in Table S3.

EIS studies were conducted using a 3 mM ferricyanide solution, as shown in Fig. 3(C), further to characterize the electrochemical properties of the modified electrodes. In EIS, the charge transfer resistance (Rct) is qualitatively indicated by the diameter of the semicircle in the Nyquist plot [32]. Rct of the modified electrodes is shown in Fig. 3(D). The bare SPE had an Rct of 5374 ± 92.7 Ω, which decreased slightly to 3687 ± 370 Ω upon addition of AMrGO layer indicating good conductivity of AMrGO. After capture probe immobilization, the Rct increased significantly to 8183 ± 277 Ω and 12,106 ± 489 Ω in the AMrGO/Cp/BSA/target/Dp/SHRP, suggesting successful immobilization of each sequential step on the developed AMrGO.

3.4. Optimizing the experimental parameters

For the best performance, the genosensor running conditions are optimized. The influence of the capture probe (Cp) and detection probe (Dp) concentrations and the hybridization times were optimized, as depicted in Fig. S4. The surface density of the capture probe was critical for the sensitivity of the biosensor. A uniform distribution of the capture probes and their optimum separation distance on the recognition layer was crucial for minimizing steric hindrance upon hybridization with the target RNA and enhancing the performance of the genosensor. The assay time includes the hybridization of target N-gene for 15 min, followed by adding a detection probe and incubating for 15 min, and adsorption of SHRP for 15 min. So the total assay time was 45 min. During optimization, only one parameter was evaluated at one time. The other five parameters (capture probe, detection probe, SHRP, blocking time, hybridization time, and detection probe incubation period) were fixed to determine the optimal setting. After the experimental parameters were optimized, the analytical performance of our sensor was evaluated under optimal conditions.

For optimization of Cp loading, different amounts of Cp (0.0625 μM to 0.5 μM) were tested. The current gradually increased with the concentration of the capture probe, and it was saturated at 0.25 μM, as noted in Fig. S4(A). The highest S/B ratio was found at 0.25 μM of Cp. Similarly, to optimize the detection probe, four concentrations between 0.0025 μM and 0.5 μM were chosen. Based on the S/B ratio, 0.25 μM of Dp was selected as the optimal concentration, as shown in Fig. S4(B).

The effect of hybridization time, which is vital for the sensitive response of the genosensor, was also investigated, as shown in Fig. S4 (C). To optimize the incubation time, 5 min, 10 min, 15 min, and 30 min were tested. The currents increased rapidly with increasing hybridization time of up to 15 min. It then leveled off at a longer incubation time, suggesting hybridized oligonucleotides formed at the electrode surface had become saturated. To improve the total assay time, the detection probe's incubation times were also tested at different times (10 min, 20 min, 30 min, and 60 min). The optimal time of the detection probe (15 min) was selected for this test, as shown in Fig. S4(D). For SHRP opti mization, various dilutions ranging from 5 × to 100 × were tested. The ΔI rose as SHRP folds increased to 25 × , then decreased. The highest S/B ratio was obtained at 25 × , as shown in Fig. S4(E). Based on the S/B ratio, 25 × was selected as the optimal dilution of SHRP.

Similarly, to optimize the H_2O_2/HQ concentrations, the 2.5/2.5 mM, 5/5 mM, 10/10 mM, and 20/20 mM were evaluated. The ΔI increased with H2O2/HQ concentration, as seen in Fig. S4(F). The highest S/B ratio occurred at 5 mM of H_2O_2 and HQ. Therefore, it was selected for future experiments. The optimization of the experimental parameters is summarized in Table S4. The blocking process significantly improves the performance of AMrGO because the blocking reagent can prevent the nonspecific binding of impurities and provide a micro-environment for target recognition. Herein, four blocking agents—fetal bovine serum (FBS), bovine serum albumin (BSA), polyethylene glycol 5000 (PEG), and dextran sulfate (DS)—were evaluated for their impact on surface protection using the S/B ratio. Based on the experimental data, BSA blocking had the highest S/ B ratio, as seen in Fig. S5. Therefore, BSA was chosen to protect the AMrGO surface and to avoid the adsorption of non-specific impurities.

3.5. Analytical performance of the genosensor

We further explored the performance of our genosensor using synthetic N-gene. The electrochemical response of the constructed genosensor to the target was measured using SWV under optimized conditions to evaluate the performance of the developed biosensor. We investigated the genosensor's performance using the synthetic N-gene of SARS-CoV-2 spiked with human saliva, urine, and serum sample. As shown in Fig. 4, the equation for the calibration curve was I (μA) = 0.388 ln (N-gene) + 5.95 for saliva, I (μA) = 0.437 ln (N-gene) + 5.64 for urine, 1.04 ln (N-gene) + 9.32 for a serum with R^2 = 0.98, 0.96, 0.98, respectively. The calculated LOD for synthetic N-genes were 0.37, 0.33, and 0.19 fM, respectively. The highest sensitivity and lowest LOD were observed in the serum sample (0.19 fM).

3.6. Estimation of the association constant and surface coverage of Cp on AMrGO

To understand the adsorption between Cp and the N-gene, we adopted the chronocoulometric method to estimate the surface coverage. The assumptions include monolayer adsorption of the target molecules and equal binding energy for all binding sites. The advantages of the EIS technique for affinity characterization include low destruction and quick measurement. The amount of Cp immobilized on the nanocomposite surface was estimated using chronocoulometry to be 1.80 × 10^{12} molecules cm^{-2} and 2.79 × 10^{12} molecules cm^{-2} after the modification with 0.0625 μM and 0.125 μM of Cp on A MrGO (Fig. S6). Our surface coverage was similar to the report of Xiao et al. also using the chronocoulometric method [33]. These results confirmed the effective coating of the capture sequence on the nanocomposite.

3.7. Sensitivity and selectivity of the genosensor

Sensitivity is another pivotal factor in evaluating the analytical performance of a biosensor. The selectivity of the developed biosensor was assessed by recording SWV responses using matched and mismatched targets. The SWV responses of the biosensor for the synthetic N-genes, mismatched targets, and random targets were investigated and shown in Fig. 5. The SWV responses for detecting the 500-fM 1-bp mismatch were almost the same as those for the blank sample. In contrast, a significant increase in the SWV response was observed for the matched target sequence. This demonstrated the excellent selectivity of the biosensor.

The sequence of the synthetic DNA target used in this study originated from the primer pair of the N gene released from CDC, USA (https://www.cdc.gov/coronavirus/2019-ncov/lab/multiplex.html). The primer can detect the conserved region of the N-2 gene, which has also been chosen by Reference [28]. We used a synthetic target N-gene containing 45-base pair for the specificity test. If a single base is wrong,

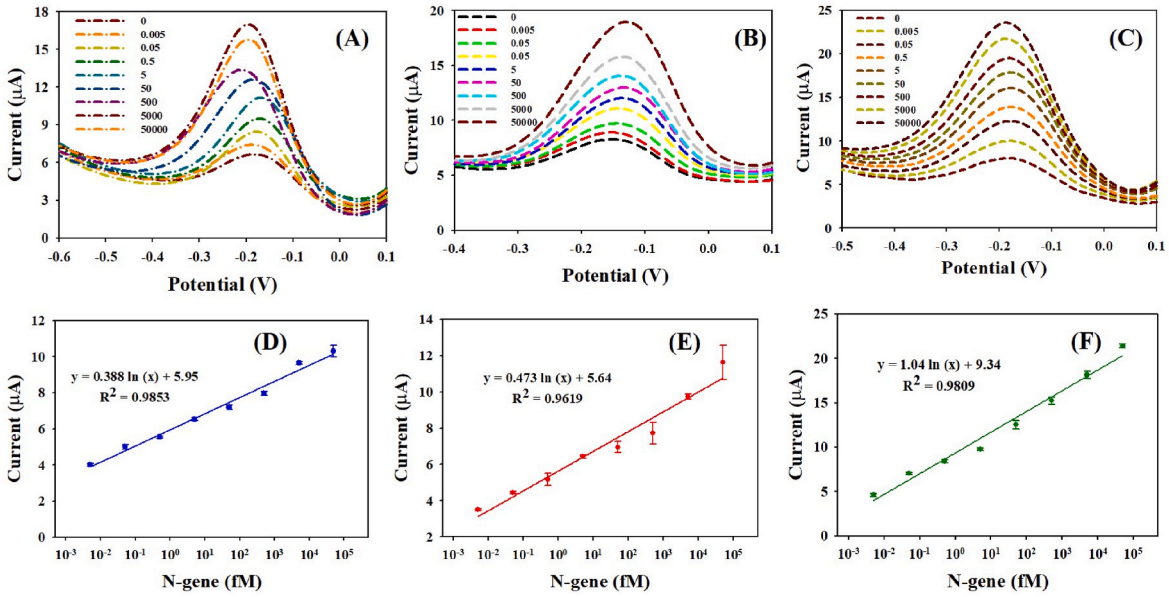

Fig. 4. (A) Square wave voltammograms of the genosensor using synthetic N-gene (5 aM–50 pM) in human saliva (A), urine (B), and serum (C). Calibration curves of the genosensor using synthetic N-gene in (D) saliva, (E) urine, and (F) serum using the genosensor. The error bar represents the standard deviation from three repeats (n = 3). SWV was run with an amplitude of 75 mV, pulse period of 100 mV, and potential range (200 mV ~ −400 mV) using 5 mM H_2O_2 as the substrate.

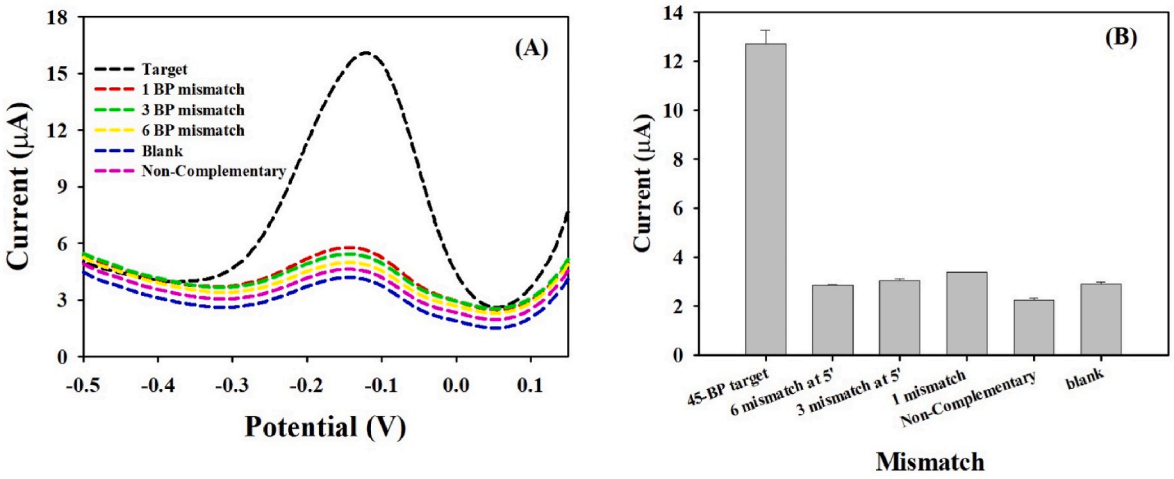

Fig. 5. The specificity of genosensor: (A)Voltammograms of different synthetic N-gene including 1bp-, 3bp-, 6bp-mismatch, random sequence, and complete matches. The used sequences were given in Table S1, (B)comparison of peak current for synthetic N-gene sequences including 1bp-, 3bp-, 6bp-mismatched, and random non-complementary sequences.

it creates a 2.2% of mismatch, which is a big difference for a short sequence. So the current of a single mismatch target (3.3 μA) was significantly lower than that of 12.71 μA from a completely matched sequence.

Furthermore, the signal intensity of the genosensors with one and two mismatches was slightly higher than those from the blank and non-complementary sequence, which indicates a low interaction between capture and signaling probes and the mismatched target sequences. The presence of the non-complementary sequence produced a signal similar to the blank, demonstrating the excellent selectivity of the biosensor to the target synthetic N-gene. Similarly, Wang et al. [11] and Zhao et al. [34] also demonstrated that a single base pair mismatch is sufficient for the signal to be comparable to a blank or random sequence (42-bp). The assay involves sandwich hybridization of N-gene with probes functionalized with redox-active labels, which are subsequently detected by square wave voltammetry (SWV). Under optimal conditions, the experiment result ensures that high specificity is achieved with the assay.

Moreover, using magnetic AMrGO to capture and separate targets from non-targets reduces the chances of carry-over contamination and pipetting error. Since the aim of our system is N-gene, we used the single capture probe to detect the target sequence in different vectors like lentivirus and amplicon from a plasmid in Supplementary Information (Fig. S7 and S8). Also, various body fluids were applied to load the N-gene of SARS-CoV-2. The N-gene from recombinant lentivirus is used as reference material for comparison.

We also compare our system with the quantitative polymerase chain reaction (QPCR) using two kinds of N-gene sequences (45-bp length and plasmid). The plasmid containing the entire N-gene from Wuhan-Hu-1 isolate of SARS-CoV-2 (GenBank: NC 045512.2) was used as a template for QPCR assay which is referred to the Kumar's publication [35]. The different concentrations of plasmid were amplified by QPCR. The

amplified fragment using N_3F and N_2R primers has the size of 550 bp. The values of quantification cycle (Cq) from QPCR amplification and plasmid concentration were used to plot Fig. S9(A). The cq value decreases with the increase in plasmid concentration in a large range of 5 aM and 10^6 aM. From the calibration curve (Fig. S9(B)), our AMrGO had the LOD of 2.4 aM and dynamic detection range of 3.36–3.36 × 10^5 aM. The analytical performance of the prepared AMrGO for the N-gene plasmid was similar to that of QPCR.

QPCR was also used to amplify and detect the synthetic N-gene (45 bp). The agarose gel electrophoresis is used to visualize the amplicon since the low fluorescence of the short amplicon cannot be used to determine Cq of QPCR. The different concentrations (0.1–1000 nM) of synthetic N-gene were amplified by QPCR and their amplicons were analyzed using agarose electrophoresis. As shown in Fig. S10(B), the ampicon has the correct size of 45 bp and clear image at lane 3 (1000 nM). The weak bands for N-gene doses (100 nM and 10 nM) are demonstrated in lane 4 and 5 in Fig. S10(B). The detection limit for the 45-bp sequence was around 10 nM using QPCR since the no amplicon was observed when N-gene concentration was less than 10 nM. The QPCR procedure shall be optimized to enhance amplification efficiency for the 45-bp gene. In contrast, the developed biosensor preserved good linear relationship in the (5 aM- 50pM) and the LOD for N-genes in saliva were 0.3 7 aM (Fig. S10(C). The developed AMrGO offers good precision and accuracy, which is especially suitable for routine studies of N-gene in different samples. In summary, the developed AMrGO was simple, inexpensive, and portable for N-gene detection, which hold great potential for point of care testing as compared to QPCR method.

3.8. Stability and storage test

We evaluated the sensing performance to check the long-term storability of the AMrGO/Cp/BSA at 4 °C for 13 weeks. The stability of the modified nanocomposites was evaluated based on the current signal and S/B ratio. The stability study (Fig. 6) showed that the genosensor retained about 80% of its detection capability at the end of 13 weeks compared to the day-1 measurement. The relative standard deviations of all measurements were within 10%. After being stored in a refrigerator for three weeks, the nanocomposites retained about 90% of their initial responses. These results suggest that our material is stable enough to be applied on the electrode surface after storage.

Electrochemical genosensors are used to detect the specific sequences of pathogenic viruses. For example, SPEs modified with thiolated DNA can detect 20-mer DNA and 280-mer RNA in various positions from the avian influenza virus. The current signals of the redox probe

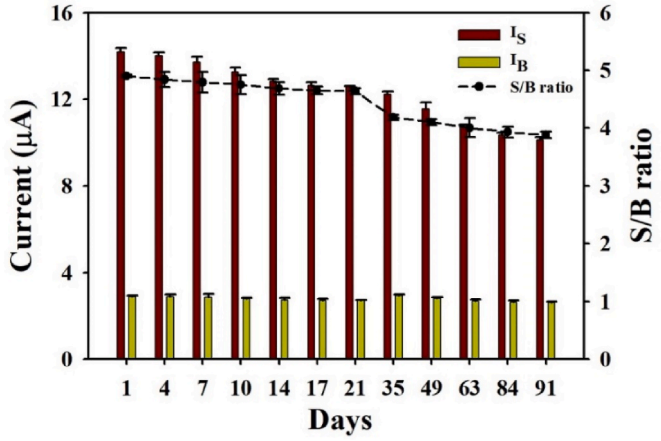

Fig. 6. Stability test of the genosensor after 91-day storage at 4 °C. SWV was run with an amplitude of 75 mV, pulse period 100 mV, and initial potential (200 mV ~ −400 mV) using 5 mM H_2O_2 as the substrate. The concentration of SARS-CoV-2 synthetic N-gene was 500 fM.

using SWV after hybridization are obtained at 1 pM of the RNA transcript [30]. Kumar et al. developed a printed circuit board electrode to monitor the amplicons of SARS-CoV-2 amplified from PCR. After the intercalator (methylene blue) is optimized, the electrode can detect 10 pg/μl (1.7 fM) of nucleocapsid amplicons [35]. A label-free DNA capacitive biosensor has been reported for detecting the RNA-dependent RNA polymerase (RdRp) gene using a biosensor composed of platinum/titanium electrodes and a DNA capture probe [36]. However, fabricating this interdigitated electrode on a glass wafer requires expensive photolithography instruments. The ORF1ab gene was selected as the target and amplified using the techniques of catalytic hairpin assembly and terminal deoxynucleotidyl transferase to generate single-stranded DNA products. The addition of a Ru probe can convert the DNA product to electrochemical signals in the target range of 0.1 pM–1000 pM with a detection limit of 26 fM using DPV [37]. Another study also detected the ORF1ab gene using molybdenum disulfide-modified SPE and a thiolated DNA probe without enzyme amplification. A thionine-carbon nanodot was used as a hybridization indicator, with a detection limit of 1.01 pM [38]. Song et al. developed electrochemical biosensors using electropolymerized polyaniline nanowires to capture DNA and antifouling peptides to detect N-gene with a low detection limit (3.5 fM) [39]. These literature reports for SARS-CoV-2 biosensors are summarized in Table 1.

In this study, the detection limit of our genosensors was comparable to the reported genosensors in the range of 1 pM–3 aM. We achieved N-gene LOD of 0.31 aM and 0.54 aM in human urine and serum, respectively. The N-gene LOD of our genosensor was smaller, and the linear range was larger compared to the previous papers [35,39]. A low-cost electrochemical genosensor based on SPE and magnetic nanocomposites from rGO was successfully developed for N genes. Based on a sandwich-type recognition, our platform was confirmed to practicably detect the N-gene of SARS-CoV-2 by using a portable electrochemical device without nucleic acid amplification and reverse transcription. Our developed platform, concerning its speed (time), and limit of detection (LOD), is better than compared literature (Table 1). Additionally, a linear response in a wide range of target concentrations and reduced influence of undesirable entities were obtained using this developed platform. Our AMGO, with the aid of a magnet, enables simple washing and easy separation on the working electrode. This platform's advantages include low cost, fast response, long-term stability, real-time diagnostic procedure, and facile assay compared to expensive PCR instruments. We demonstrated rapid electrochemical analysis of N-gene with acceptable sensitivity and high specificity, which can potentially be used for point-of-care diagnostics. All the samples were used directly for detection without amplification and reverse transcription. The magneticity of AMrGO results in efficient gene capture, separation, and signal amplification onto the printed electrode and reduces the chances of carry-over contamination and pipetting error.

Moreover, the detection limit is comparable to or even better than the published SARS-CoV-2 genosensors (Table 1). Compared with the intercalator method [35], the developed biosensor presents a lower detection limit. However, some challenges must still be carefully investigated in future studies. No clinical samples from SARS-CoV-2 patients were used. Since an SPE has a 2-year shelf life, the stability of the detection nanocomposite must extend to 2 years of storage by optimizing the blocking process and stabilizing the DNA structure for future commercial applications.

4. Conclusion

A facile protocol for synthesizing and modifying a nanocomposite is reported here. An AMrGO nanocomposite and SPE were used to fabricate a genosensor for the highly sensitive and selective detection of the viral N-gene. The nanocomposite has a large surface area and good magnetic separation and is easily synthesized and modified. We provided evidence of the rapid analysis of the N-gene added to human

Table 1
Electrochemical DNA biosensors for SARS-CoV-2.

Gene	Recognition element	Detection element	Linear range	LOD	Assay time (min)	Electrochemical method	Ref.
ORF1ab	Hairpin DNA probes, gold electrode	Terminal deoxynucleotidyl transferase, $Ru(NH_3)_6$	0.1–1000 pM	26 fM	180	DPV	[31]
ORF1ab	MoS2, SPE, DNA probe	thionine-carbon nanodot	–	1.01 pM	90	DPV	[32]
N-gene	Electropolymerized polyaniline, GCE, peptides, DNA probe	–	10-1000000 fM	3.5 fM	60	DPV	[33]
ORF1ab	Au@Fe_3O_4, SPE, DNA probe, calixarene-GO	toluidine blue	0.01–1000 fM	3 aM	180	DPV	[34]
N-gene amplicon	printed circuit board, PCR	methylene blue	–	1.7 fM	60	DPV	[28]
ORF1ab fragment of SARS-CoV-2 RNA	AuNMs and CDs	$[Ru (bpy)3]^{2+}$	50 fM-100 nM	514 aM		ECL	[40]
N-gene	AMrGO	H_2O_2/SHRP	5 aM–50 pM	0.37 fM (Saliva) 0.33 fM (Urine) 0.19 fM (Serum)	45	SWV	This study

serum and saliva. The advantages of the developed genosensor include a low-cost, disposable electrode and a low LOD of 0.37 fM. The most important aspect is that the assay is quick (within 45 min of detection time) and capable of providing quantitative measurement. The developed genosensors showed good storage stability and reproducibility for up to 13 weeks.

Credit author statement

Data curation, Pravanjan Malla, Pinpinut Kabinsing; Investigation, Pravanjan Malla, Chi-Hsien Liu; Methodology, Wei-Chi Wu and Chi-Hsien Liu; Resources, Wei-Chi Wu and Chi-Hsien Liu; Writing, Pravanjan Malla, Chi-Hsien Liu, Paiboon Sreearunothai.

All authors have read and agreed to the published version of the manuscript.

Declaration of competing interest

The authors declare that they have no known competing financial interests or personal relationships that could have appeared to influence the work reported in this paper.

Data availability

No data was used for the research described in the article.

Acknowledgments

We express gratitude to Ministry of Science and Technology (111-2221-E-182-016), Chang Gung University (BMRP 758), and Chang Gung Memorial Hospital (CMRPD 1M0601, 1M0681) for funding and supporting this research. The authors thank the Instrumentation Center and Microscopy Center @CGU and Yung-Sheng Chen @NSCRIC in NTHU for SQUID analysis.

References

[1] N. Kumar, N.P. Shetti, S. Jagannath, T.M. Aminabhavi, Electrochemical sensors for the detection of SARS-CoV-2 virus, Chem. Eng. J. 430 (2022), 132966.
[2] T. Chaibun, J. Puenpa, T. Ngamdee, N. Boonapatcharoen, P. Athamanolap, A. P. O'Mullane, S. Vongpunsawad, Y. Poovorawan, S.Y. Lee, B. Lertanantawong, Rapid electrochemical detection of coronavirus SARS-CoV-2, Nat. Commun. 12 (1) (2021) 802.
[3] L. Wu, X. Wang, C. Wu, X. Cao, T. Tang, H. Huang, X. Huang, Ultrasensitive SARS-CoV-2 diagnosis by CRISPR-based screen-printed carbon electrode, Anal. Chim. Acta 1221 (2022), 340120.
[4] H.F. El Sharif, S.R. Dennison, M. Tully, S. Crossley, W. Mwangi, D. Bailey, S. P. Graham, S.M. Reddy, Evaluation of electropolymerized molecularly imprinted polymers (E-MIPs) on disposable electrodes for detection of SARS-CoV-2 in saliva, Anal. Chim. Acta 1206 (2022), 339777.
[5] M.M. Islam, D. Koirala, Toward a next-generation diagnostic tool: a review on emerging isothermal nucleic acid amplification techniques for the detection of SARS-CoV-2 and other infectious viruses, Anal. Chim. Acta 1209 (2022), 339338.
[6] G. Martins, J.L. Gogola, L.H. Budni, M.A. Papi, M.A.T. Bom, M.L.T. Budel, E.M. de Souza, M. Müller-Santos, B.C.B. Beirão, C.E. Banks, L.H. Marcolino-Junior, M. F. Bergamini, Novel approach based on GQD-PHB as anchoring platform for the development of SARS-CoV-2 electrochemical immunosensor, Anal. Chim. Acta 1232 (2022), 340442.
[7] L.C. Brazaca, P.L. dos Santos, P.R. de Oliveira, D.P. Rocha, J.S. Stefano, C. Kalinke, R.A. Abarza Muñoz, J.A. Bonacin, B.C. Janegitz, E. Carrilho, Biosensing strategies for the electrochemical detection of viruses and viral diseases – a review, Anal. Chim. Acta 1159 (2021), 338384.
[8] D. Alzate, M.C. Lopez-Osorio, F. Cortés-Mancera, M.C. Navas, J. Orozco, Detection of hepatitis E virus genotype 3 in wastewater by an electrochemical genosensor, Anal. Chim. Acta 1221 (2022), 340121.
[9] G. Darabdhara, M.R. Das, S.P. Singh, A.K. Rengan, S. Szunerits, R. Boukherroub, Ag and Au nanoparticles/reduced graphene oxide composite materials: synthesis and application in diagnostics and therapeutics, Adv. Colloid Interface Sci. 271 (2019), 101991.
[10] M.H. Choi, J. Lee, Y.J. Seo, Combined recombinase polymerase amplification/rkDNA–graphene oxide probing system for detection of SARS-CoV-2, Anal. Chim. Acta 1158 (2021), 338390.
[11] X. Wang, Y. Li, M. Zhao, H. Wang, Q. Wan, C. Shi, C. Ma, An ultrafast ratiometric electrochemical biosensor based on potential-assisted hybridization for nucleic acids detection, Anal. Chim. Acta 1211 (2022), 339915.
[12] M. Sharafeldin, J.J. Davis, Characterising the biosensing interface, Anal. Chim. Acta 1216 (2022), 339759.
[13] C. Ingrosso, M. Corricelli, F. Bettazzi, E. Konstantinidou, G.V. Bianco, N. Depalo, M. Striccoli, A. Agostiano, M.L. Curri, I. Palchetti, Au nanoparticle: in situ decorated RGO nanocomposites for highly sensitive electrochemical genosensors, J. Mater. Chem. B 7 (5) (2019) 768–777.
[14] B. Khalilzadeh, N. Shadjou, H. Afsharan, M. Eskandani, H.N. Charoudeh, M. R. Rashidi, Reduced graphene oxide decorated with gold nanoparticle as signal amplification element on ultra-sensitive electrochemiluminescence determination of caspase-3 activity and apoptosis using peptide based biosensor, Bioimpacts 6 (3) (2016) 135–147.
[15] S.R. Ahmed, K. Takemeura, T.C. Li, N. Kitamoto, T. Tanaka, T. Suzuki, E.Y. Park, Size-controlled preparation of peroxidase-like graphene-gold nanoparticle hybrids for the visible detection of norovirus-like particles, Biosens. Bioelectron. 87 (2017) 558–565.
[16] X. Cao, Z. Xia, W. Yan, S. He, X. Xu, Z. Wei, Y. Ye, H. Zheng, Colorimetric biosensing of nopaline synthase terminator using Fe3O4@Au and hemin-functionalized reduced graphene oxide, Anal. Biochem. 602 (2020), 113798.
[17] M. Fani, M. Rezayi, Z. Meshkat, S.A. Rezaee, M. Makvandi, K. Ahmadi Angali, A novel electrochemical DNA biosensor based on a gold nanoparticles-reduced graphene oxide-polypyrrole nanocomposite to detect human T-lymphotropic virus-1, IEEE Sensor. J. 20 (18) (2020) 10625–10632.
[18] Y. Zhang, C. Pilapong, Y. Guo, Z. Ling, O. Cespedes, P. Quirke, D. Zhou, Sensitive, simultaneous quantitation of two unlabeled DNA targets using a magnetic nanoparticle–enzyme sandwich assay, Anal. Chem. 85 (19) (2013) 9238–9244.
[19] P. Malla, H.P. Liao, C.H. Liu, W.C. Wu, P. Sreearunothai, Voltammetric biosensor for coronavirus spike protein using magnetic bead and screen-printed electrode for point-of-care diagnostics, Microchim. Acta 189 (4) (2022) 168.
[20] Q. Zhang, L. Li, Z. Qiao, C. Lei, Y. Fu, Q. Xie, S. Yao, Y. Li, Y. Ying, Electrochemical conversion of Fe3O4 magnetic nanoparticles to electroactive prussian blue analogues for self-sacrificial label biosensing of avian influenza virus H5N1, Anal. Chem. 89 (22) (2017) 12145–12151.
[21] G. Wu, S. Yan, Reasoning of spike glycoproteins being more vulnerable to mutations among 158 coronavirus proteins from different species, J. Mol. Model. 11 (1) (2005) 8–16.

[22] D.K. Agarwal, V. Nandwana, S.E. Henrich, V.P.V.N. Josyula, C.S. Thaxton, C. Qi, L. M. Simons, J.F. Hultquist, E.A. Ozer, G.S. Shekhawat, V.P. Dravid, Highly sensitive and ultra-rapid antigen-based detection of SARS-CoV-2 using nanomechanical sensor platform, Biosens. Bioelectron. 195 (2022), 113647.
[23] L.S. Jung, T.M. Gund, M. Narayan, Comparison of binding site of remdesivir and its metabolites with NSP12-NSP7-NSP8, and NSP3 of SARS CoV-2 virus and alternative potential drugs for COVID-19 treatment, Protein J. 39 (6) (2020) 619–630.
[24] X. Zhang, M. Li, B. Zhang, T. Chen, D. Lv, P. Xia, Z. Sun, X. Shentu, H. Chen, L. Li, W. Qian, The N gene of SARS-CoV-2 was the main positive component in repositive samples from a cohort of COVID-19 patients in Wuhan, China, Clin. Chim. Acta 511 (2020) 291–297.
[25] D.C. Marcano, D.V. Kosynkin, J.M. Berlin, A. Sinitskii, Z. Sun, A. Slesarev, L. B. Alemany, W. Lu, J.M. Tour, Improved synthesis of graphene oxide, ACS Nano 4 (8) (2010) 4806–4814.
[26] Y. Wang, X. Wu, W. Zhang, S. Huang, Synthesis and electromagnetic absorption properties of Ag-coated reduced graphene oxide with MnFe2O4 particles, J. Magn. Magn Mater. 404 (2016) 58–63.
[27] G.-C. Chen, C.-H. Liu, W.-C. Wu, Electrochemical immunosensor for serum parathyroid hormone using voltammetric techniques and a portable simulator, Anal. Chim. Acta 1143 (2021) 84–92.
[28] H. Hosseini, H. Ahmar, A. Dehghani, A. Bagheri, A.R. Fakhari, M.M. Amini, Au-SH-SiO2 nanoparticles supported on metal-organic framework (Au-SH-SiO2@Cu-MOF) as a sensor for electrocatalytic oxidation and determination of hydrazine, Electrochim. Acta 88 (2013) 301–309.
[29] S. Wang, F. Yang, D. Jin, Q. Dai, J. Tu, Y. Liu, Y. Ning, G.J. Zhang, Toehold mediated one-step conformation-switchable "signal-On" electrochemical DNA sensing enhanced with homogeneous enzymatic amplification, Anal. Chem. 89 (10) (2017) 5349–5356.
[30] K. Malecka, A. Stachyra, A. Góra-Sochacka, A. Sirko, W. Zagórski-Ostoja, H. Radecka, J. Radecki, Electrochemical genosensor based on disc and screen printed gold electrodes for detection of specific DNA and RNA sequences derived from Avian Influenza Virus H5N1, Sensor. Actuator. B Chem. 224 (2016) 290–297.
[31] J. Dong, H. Yang, J. Zhao, L. Wen, C. He, Z. Hu, J. Li, D. Huo, C. Hou, Sandwich-type microRNA biosensor based on graphene oxide incorporated 3D-flower-like MoS2 and AuNPs coupling with HRP enzyme signal amplification, Microchim. Acta 189 (1) (2022) 49.
[32] J. Ma, W. Bai, J. Zheng, A novel self-cleaning electrochemical biosensor integrating copper porphyrin-derived metal-organic framework nanofilms, G-quadruplex, and DNA nanomotors for achieving cyclic detection of lead ions, Biosens. Bioelectron. 197 (2022), 113801.
[33] Q. Xiao, J. Li, X. Jin, Y. Liu, S. Huang, Ultrasensitive electrochemical microRNA-21 biosensor coupling with carboxylate-reduced graphene oxide-based signal-enhancing and duplex-specific nuclease-assisted target recycling, Sens. Actuators, B 297 (2019), 126740.
[34] H. Zhao, F. Liu, W. Xie, T.-C. Zhou, J. OuYang, L. Jin, H. Li, C.-Y. Zhao, L. Zhang, J. Wei, Y.-P. Zhang, C.-P. Li, Ultrasensitive supersandwich-type electrochemical sensor for SARS-CoV-2 from the infected COVID-19 patients using a smartphone, Sensor. Actuator. B Chem. 327 (2021), 128899.
[35] M.S. Kumar, R. Nandeshwar, S.B. Lad, K. Megha, M. Mangat, A. Butterworth, C. W. Knapp, M. Knapp, P.A. Hoskisson, D.K. Corrigan, A.C. Ward, K. Kondabagil, S. Tallur, Electrochemical sensing of SARS-CoV-2 amplicons with PCB electrodes, Sens. Actuators, B 343 (2021), 130169.
[36] C. Hwang, N. Park, E.S. Kim, M. Kim, S.D. Kim, S. Park, N.Y. Kim, J.H. Kim, Ultra-fast and recyclable DNA biosensor for point-of-care detection of SARS-CoV-2 (COVID-19), Biosens. Bioelectron. 185 (2021), 113177.
[37] Y. Peng, Y. Pan, Z. Sun, J. Li, Y. Yi, J. Yang, G. Li, An electrochemical biosensor for sensitive analysis of the SARS-CoV-2 RNA, Biosens. Bioelectron. 186 (2021), 113309.
[38] E. Martínez-Periñán, T. García-Mendiola, E. Enebral-Romero, R. del Caño, M. Vera-Hidalgo, M. Vázquez Sulleiro, C. Navío, F. Pariente, E.M. Pérez, E. Lorenzo, A MoS2 platform and thionine-carbon nanodots for sensitive and selective detection of pathogens, Biosens. Bioelectron. 189 (2021), 113375.
[39] Z. Song, Y. Ma, M. Chen, A. Ambrosi, C. Ding, X. Luo, Electrochemical biosensor with enhanced antifouling capability for COVID-19 nucleic acid detection in complex biological media, Anal. Chem. 93 (14) (2021) 5963–5971.
[40] L. Gutiérrez-Gálvez, R. del Caño, I. Menéndez-Luque, D. García-Nieto, M. Rodríguez-Peña, M. Luna, T. Pineda, F. Pariente, T. García-Mendiola, E. Lorenzo, Electrochemiluminescent nanostructured DNA biosensor for SARS-CoV-2 detection, Talanta 240 (2022), 123203.